Realization of single-layer Fourier phased metasurfaces for wideband RCS reduction

https://doi.org/10.1109/lawp.2023.3235970

PUBLISHER

Institute of Electrical and Electronics Engineers (IEEE)

VERSION

AM (Accepted Manuscript)

Realization of Single Layer Fourier Phased Metasurfaces for Wideband RCS Reduction

Mustafa K. Taher Al-Nuaimi, *Senior Member, IEEE,* Guan-Long Huang, *Senior Member, IEEE,* William G. Whittow, *Senior Member*, *IEEE*, Rui-Sen Chen, *Member*, *IEEE*, *Sai*-Wai Wong

***Abstract*— An efficient and fast strategy to design and realize single layer Fourier phased metasurfaces for wideband radar cross section (RCS) reduction when illuminated by a circular polarization (CP) plane wave is proposed in this letter. The scattering phase (between 0º and 360º) required at each unit cell of the proposed metasurfaces was computed using the Fourier phase formula in which the focal length (*F*) is inversely proportional to the phase distribution. Pancharatnam-Berry (PB) phase theory was applied with unit cells of subwavelength periodicity to further enhance the scattering and RCS reduction characteristics. The proposed wideband Fourier phased metasurface has a square shape and contains 30 × 30 PB unit cells with subwavelength periodicity of 5 mm ≈ 0.26λ_{16GHz}. Both simulation and measured results show that the proposed Fourier phased metasurfaces can achieve more than 10 dB of RCS reduction under normal incidence of CP plane wave regardless of the value of *F*. Under oblique incidence, more than 10 dB of RCS reduction was maintained for incident angles up to 60°. In addition, the single-layer Fourier phased metasurface features wideband 10 dB RCS reduction bandwidth from 10 GHz to 24 GHz with a thickness of only 2 mm. This resulted in an 82.3% fractional bandwidth (FBW) of RCS reduction which is higher than other designs reported in the literature. The proposed design strategy provides a promising way to design and realize metasurfaces for wideband and stable RCS reduction performance without the need to use a computationally complex and/or time-consuming and slow running optimization algorithm.**

***Index Terms*— Fourier phase, radar cross section, radar, metasurface, reflectarray, antenna array.**

I. INTRODUCTION

Metasurfaces are a 2D engineered surface which can be used to manipulate the phase, magnitude, and polarization of the incident electromagnetic wave (EM-wave) and therefore achieve extraordinary functionalities such as polarization conversion [1] – [5], beam steering [6], beam focusing [7] – [8], cloaking [9]–[10]..etc. Radar cross section (RCS) and diffusion of EM waves is one of the important functions of the metasurface and has been a hot topic in the last decade [11] – [15]. Chessboard and checkerboard metasurfaces are among the first metasurfaces designs for RCS reduction [16]–[19]. Even though they have good boresight RCS reduction characteristics, their scattering patterns have strong reflection in some directions. In addition, the scattering characteristics of the chessboard and checkerboard metasurfaces are degraded severely under oblique incidence of EM plane wave. To overcome the drawbacks associated with chessboard and checkerboard metasurfaces, coding metasurfaces was proposed in [20] to realize diffusive scattering and to provide an extraordinary freedom for manipulating EM-waves. However, the diffused scattering of the coding metasurface cannot be ensured without using a complicated and time-consuming algorithm for massive optimizations (sometimes prohibitive) to find the optimum 1-bit, 2-bit, or multibit phase distribution, which necessitates plenty of computational computer resources [21]–[22]. In addition, ensuring wideband RCS reduction under wide-angles of incidence is not an easy task. Moreover, time-consuming algorithms are quite complicated for layman users to design coding metasurfaces as plenty of specialized knowledge in those complicated optimization algorithms are required. In addition, the absence of a design formula that can be used to achieve the optimum phase distribution required for more than 10 dB RCS reduction make the design and realization of metasurface is much harder [23] – [27].

Fourier phase formula has been used recently to design a metalens for EM-wave focusing and for beam scanning [28] – [30]. To the authors' best knowledge, the scattering performance and RCS reduction of metasurfaces designed using Fourier phase distribution has never been explored before. This letter presents an efficient technique based on 2D Fourier phase formula and Pancharatnam-Berry (PB) theory to design diffusive metasurfaces with wideband RCS reduction under both normal and oblique incidence of EM plane wave. The proposed technique makes the design process more efficient less time-consuming and without the need to use complicated optimization algorithms to find the optimum phase distribution.

II. PB UNIT CELL DESIGN AND RESULTS

In order to design a metasurface with a wideband characteristic, a unit cell with a wideband reflection characteristic is required. The configuration of the proposed PB unit cell in this study is shown in Fig. 1(a). The unit cell consists of a dielectric substrate (ε_r = 4.4, h = 2 mm) sandwiched between two copper layers.

Manuscript received March XX, XXXX; revised March XX, XXXX; accepted March XX, XXXX. Date of publication March XX, XXXX; date of current version XX, XXXX. (Corresponding author: G. L. Huang). This work was part supported in part by grant no. K202317 of the State Key Laboratory of Millimeter waves, Southeast University, China. Newton International Fellowship grant no. NIF\R1\222093 by The Royal Society, UK. EPSRC grant 'ANISAT', EP/S030301/1.

M. K. T. Al-Nuaimi, G. L. Huang, R.-S. and Chen are with School of AI-Guangdong & Taiwan, Foshan University, Foshan 528225, China; (e-mail:mustafa.engineer@yahoo.com, hgl@fosu.edu.cn, crs@ fosu.edu.cn).

M. K. T. Al-Nuaimi is with the State Key Laboratory of Millimeter waves, Southeast University, China.

M. K. T. Al-Nuaimi and W. G. Whittow are with the Wolfson School of Mechanical, Electrical and Manufacturing Engineering, Loughborough University, Loughborough LE113TU, U.K. (e-mail: M.Al-Nuaimi@lboro.ac.uk, w.g.whittow@lboro.ac.uk).

S.-W. Wong is with College of Electronics and Information Engineering, Shenzhen University, Shenzhen 518060, China.

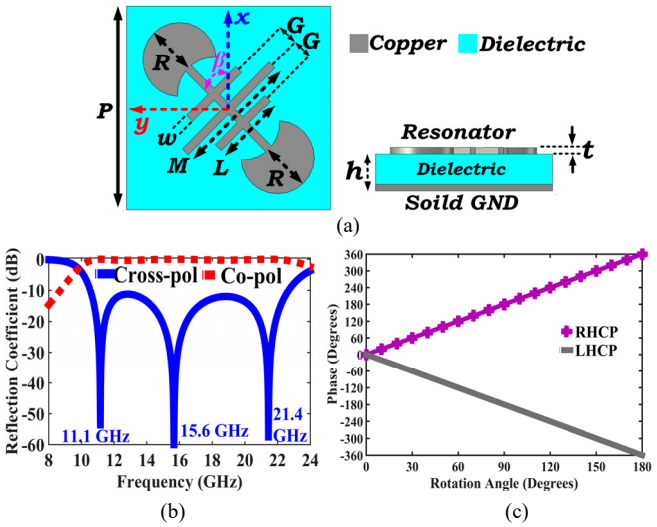

Fig. 1. (a) Top and side views of the PB unit cell. (b) Simulated magnitudes of the co-pol and cross-pol reflection components under CP plane wave illumination. (c) Reflection phase of the co-pol component for various rotation angles (β) of the resonator versus frequency.

The thickness of the copper layer was set as t = 0.018 mm. The upper copper layer is composed of the resonator shown in Fig. 1(a) with a full metal ground plane (bottom layer). The PB unit cell periodicity was selected as P = 5 mm, which is equivalent to 0.26λ_o at 16 GHz. The optimized physical parameters of the unit cell are L = 1.6 mm, M = 3 mm, G = 0.5 mm, w = 0.2 mm, and R = 0.8 mm. The reflection characteristics of the PB unit cell were achieved using CST Microwave Studio with unit cell boundary conditions along both ±x and ±y directions. Excitation ports were assigned in the ±z directions. The simulated magnitudes of the co-polarized (co-pol) and cross-polarized (cross-pol) reflected components under circularly polarized (CP) plane wave excitation is shown in Fig. 1(b). The magnitude of the co-pol component is close to 0 dB, which means a very high level of reflection. On the other hand, the magnitude of the cross-pol component is kept less than −11 dB over a wide frequency band from 10.2 GHz to 23.6 GHz (FBW = 79.3%) and reached more than −50 dB at resonance frequencies. In addition, it can be noted that the unit cell has three resonance frequencies at 11.1 GHz, 15.6 GHz, and 21.4 GHz as a result of the parallel and antiparallel current distributions according to Faraday's law [31]. Based on the reflection component results and according to PB phase theory [32], the reflection phase ($\phi_{\text{co-pol}}$) of the co-pol component will be a function to the rotation angle (β) of the copper resonator and related to each other as $\phi_{\text{co-pol}} = \pm 2\beta$. The '+' and '−' denote the right-hand circular polarization (RHCP) and left-hand circular polarization (LHCP) incident waves. When β (rotation angle) gradually increased from 0° to 180°, the $\phi_{\text{co-pol}}$ range is between ±180° over the frequency band from 10 GHz to 24 GHz. Thus, any desired reflection phase value across the proposed metasurface aperture can be achieved by rotating the unit cell to the desired angle. The key motivation of using a wideband PB unit cell is to make the Fourier metasurface insensitive the polarization of the incident wave (over a wide frequency band) which is highly needed for the radar stealth applications when the polarization of the incoming EM plane wave is usually unknown.

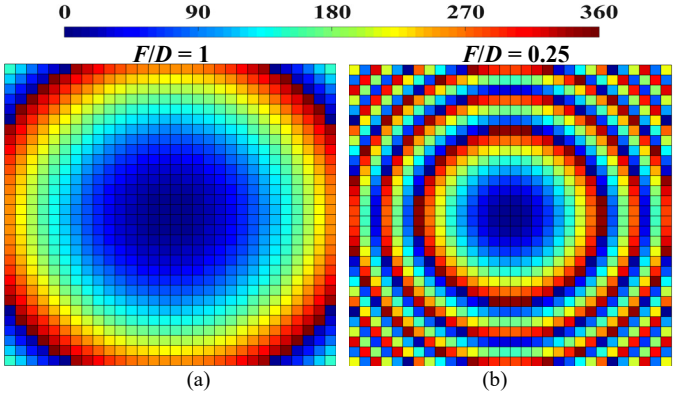

Fig. 2. Fourier phase distribution of the metasurfaces calculated using equation (1) for (a) F/D = 1 and (b) F/D = 0.25. Where D is the aperture dimension of the metasurface and D = 150 mm.

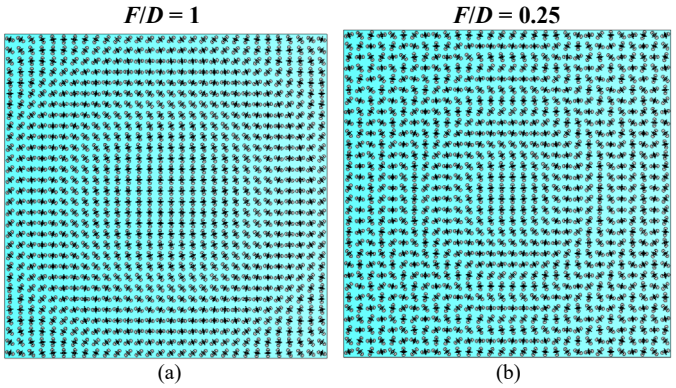

Fig. 3. Designed Fourier phased metasurfaces for (a) F/D = 1 and (b) F/D = 0.25. Where D is the aperture dimension of the metasurface and D = 150 mm. The metasurface consists of 30 × 30 PB unit cells.

III. Fourier Phased Metasurface Design

The proposed design technique is based on using Fourier phase formula for direct calculation of the phase distribution and to design RCS reducer metasurfaces without the need to use any complicated or time-consuming algorithms. The first step in the design of the proposed Fourier phased metasurfaces is to calculate the 2D Fourier phase using equation (1) [29].

$$\phi(x,y)=\frac{k\times r^2}{2\times F}=\frac{\pi}{\lambda_o\times F}\times\left[\sqrt{X_c^{\,2}+Y_c^{\,2}}\right]^2,\quad \phi(x,y)\alpha\frac{1}{F} \qquad (1)$$

In equation (1), k is the free space wave number, F is the focal length (the distance from the focal point to the metasurface center), λ_o is the free space wavelength at 16 GHz, X_c and Y_c denotes the center of the PB unit cell in the xy-plane. As can be seen in equation (1), the focal length F is inversely proportional to the scattering phase distribution, which is an opposite case to the conventional parabolic phase distribution in which F is directly proportional [27]. Based on equation (1), an in-house MATLAB script has been used to calculate the phase distribution of a 2D Fourier metasurfaces consisting of 30 × 30 PB unit cells. To understand the effect F on the Fourier phase distribution and the scattering characteristics, four Fourier phase distributions have been calculated with the aid of equation (1) for F/D =1, 0.75, 0.5, and 0.25 with D = 150 mm as shown in Fig. 2 (only phase distributions with F/D =1 and 0.25 are shown for brevity). Based on those Fourier phase distributions, four metasurfaces were designed (only F/D =1

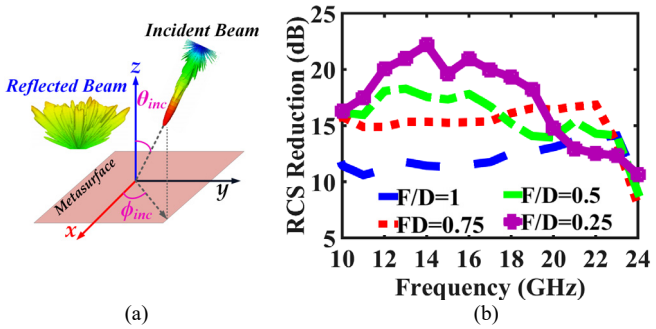

(a) (b)

Fig. 4. (a) Clarification of tha angles used in this work. (b) Simulated RCS reduction curves of the four Fourier phased metasurfaces under normal incidence of CP plane wave.

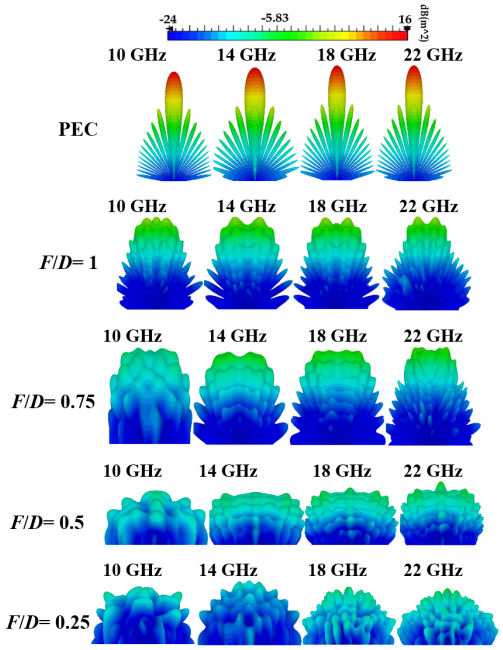

Fig. 5. The simulated 3-D far-field scattering patterns of the four Fourier phased metasurfaces at various frequencies under normal incidence of a CP plane wave.

and 0.25 metasurfaces are presented for brevity) as shown in Fig. 3. To evaluate the RCS reduction performance of the Fourier phased metasurfaces, a series of full-wave simulations were conducted using the time-domain solver in CST Microwave Studio. The metasurface was placed in the *xy*-plane and clarification of the angles used in this work are shown in Fig. 4(a) and the simulated RCS reduction curves of the four metasurfaces are presented in Fig. 4(b) under normal incidence (θ_{inc} = 0º). Compared with copper plates of the same size, all Fourier metasurfaces achieved more than 10 dB RCS reduction regardless of the *F* value over the frequency band from 10 GHz to 24 GHz resulting in a fractional bandwidth (*FBW*)= 82.3%. The mechanism of achieving such a wide RCS reduction bandwidth is due to two reasons: (1) using highly reflective unit cells of sub-wavelength periodicity and wideband operation, and (2) Fourier phase in which *F* is inversely related to the phase distribution. For a such phase distribution, an incident plane wave radiated from a source placed at *F* will be focused. But, if that plane wave is coming from a far-field region, then it will be severely diffused. To further validate the RCS reduction characteristic of the Fourier metasurfaces, the 3D scattering patterns were computed and depicted in Fig. 5 at four different

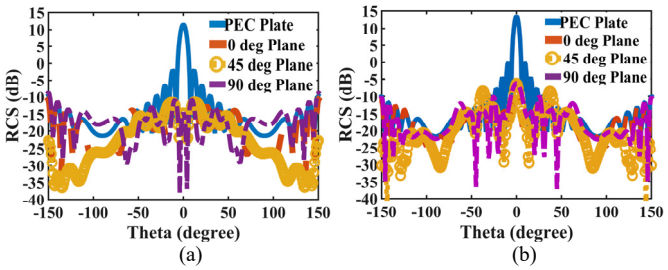

(a) (b)

Fig. 6. Simulated Cartesian scattering patterns under normal incidence of CP plane wave (θ_{inc} = 0º) of the *F/D* = 0.25 metasurface placed in the *xy*-plane at (a) 14 GHz and (b) 20 GHz for ϕ_{inc} = 0º, 45 º and 90º planes.

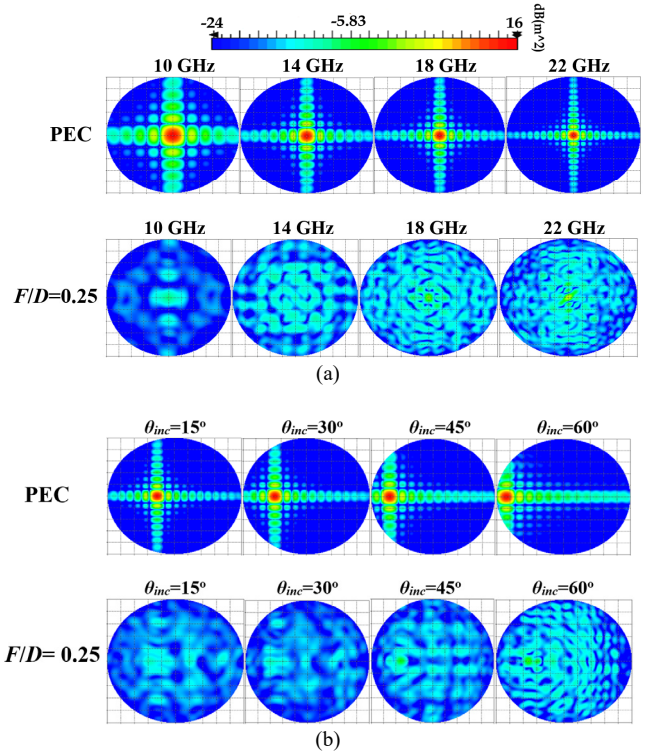

(a)

(b)

Fig. 7. Simulated (a) 2D far-field scattering distribution in front of the *F/D*=0.25 metasurface and PEC plate under normal incidence of CP plane wave (θ_{inc} = 0º, ϕ_{inc} = 0º). (b) 2D scattering distribution in the *xoy*-plane of the *F/D*=0.25 metasurface and bare PEC plate under oblique incidence.

frequencies. The 3D scattering patterns results prove that the incident CP plane wave is severely diffused and reflected back to countless directions instead of a single directive lobe reflected in the boresight direction with a PEC plate. However, it is noticed that for F/D=1 and 0.75, the scattering patterns are narrow and not very well diffused over the whole plane in front of the metasurface. As the Fourier metasurface with *F/D* = 0.25 shows a better RCS reduction level and scattering pattern shape compared to other three metasurfaces (see Figs. 4 and 5), thus the Fourier metasurface with *F/D*=0.25 will be further investigated in the rest of this letter. The Cartesian far-field scattering patterns of this metasurface was computed and presented in Fig. 6 along with those of a bare PEC plate for comparisons. It can be seen that a PEC plate has a strong reflection lobe in the boresight direction, as stated by Snell's law of reflection. However, a significant RCS reduction in the backward direction can be seen over all angles in the plane in front of the Fourier metasurface as confirmed by the 2D scattering plots in Fig. 7(a). The backscattered energy was severely diffused and distributed on the *xoy*-plane in front of the

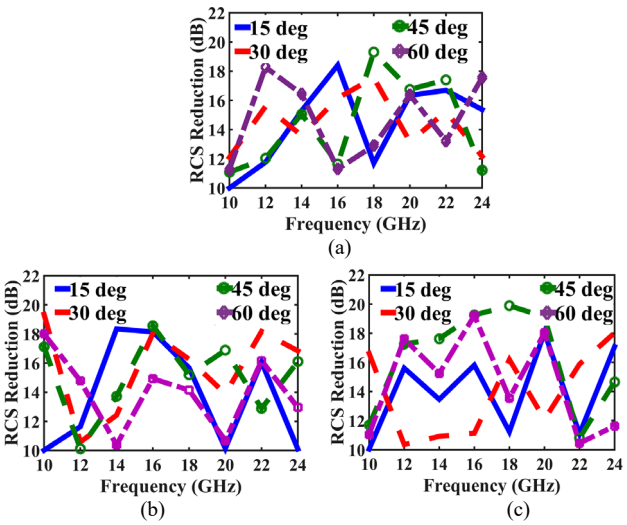

Fig. 8. The RCS reduction under oblique incidence of CP plane wave for θ_{inc} = 15°, 30°, 45°, and 60° when (b) ϕ_{inc} =0°, (c) ϕ_{inc} =45°, and (d) ϕ_{inc} =90°.

metasurface and the directive lobe which appears as a red spot for the PEC plate case has been reduced. These results demonstrate the capability of the Fourier metasurface for RCS reduction. The RCS reduction characteristics of the *F/D*=0.25 Fourier phased metasurface was further investigated under oblique incidence of CP plane wave when θ_{inc} increased from 15° to 60° as shown in Fig. 7(b). In a PEC plate case, the angles of incidence and reflection are equal according to Snell's law of reflection and the reflected beam can be clearly seen as a red spot at $\theta_{inc} = \theta_{reflected}$. For the *F/D* = 0.25 Fourier phased metasurface the scattered energy is severely diffused into countless angles with $\theta_{inc} \neq \theta_{reflected}$. The RCS reduction was further investigated under oblique incidence for ϕ_{inc} = 0°, 45°, and 90° planes and θ_{inc} increased from 15° to 60° and the results are presented in Fig. 8. It is noticed that the RCS reduction magnitude is always more than 10 dB for all angles. These results confirm that the presented design approach is robust and the ability of the Fourier metasurfaces using direct design formula to efficiently achieve more than 10 dB of RCS reduction without using any complicated optimization algorithms.

IV. Fabrication and Experimental Results

For experimental verification, a prototype of the proposed *F/D* = 0.25 Fourier metasurface was fabricated using standard PCB technology. The overall dimensions of the fabricated sample is 150 mm × 150 mm as shown in Fig. 9(a). A sketch of the measurement setup used for the RCS reduction measurement is shown in Fig. 9(b) which consists of two identical horn antennas one for transmitting waves and the other one for collecting the backscattered waves. The horn antennas were placed symmetrically and close to each other and, at the same time, far enough from the metasurface under test at a distance *R* to satisfy the far-field formula [33]. Both simulated and measured monostatic RCS results are normalized to a copper plate with the same dimensions and plotted in Fig. 9(c). It can be seen that more than 10 dB of RCS reduction was achieved from 10 – 24 GHz. A small discrepancy between the measured and simulated results were observed, which is a result of the fabrication tolerance, and misalignment of the antennas during the measurements. The proposed Fourier metasurface was compared to other designs in the literature as listed in Table I. The Fourier phased metasurface demonstrated a wider RCS reduction bandwidth (FBW) under oblique incidence up to 60°.

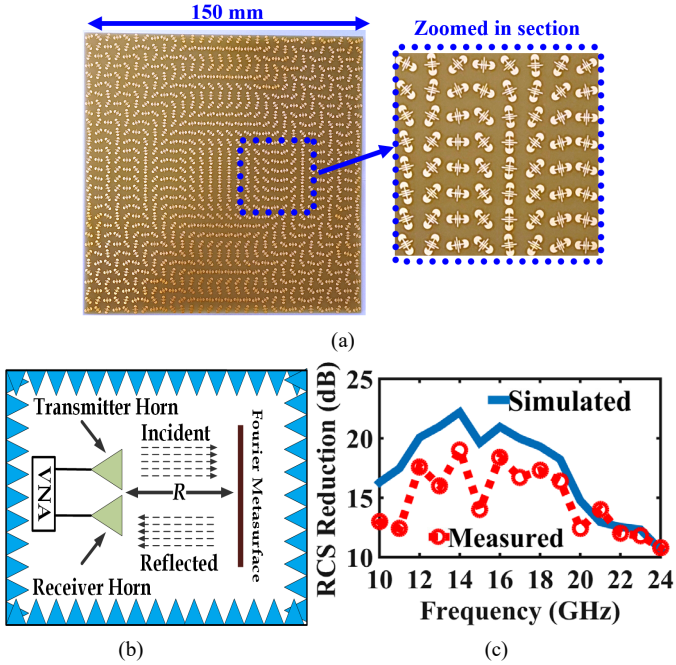

Fig. 9. (a) Photo of the fabricated prototype, (b) RCS measurement setup, and (c) the measured and simulated RCS reduction curves compared to the same sized copper plate.

TABLE I
Comparison of This Work With Previous Works

Ref.	Surface Type	10-dB RCS BW (GHz)	FBW (%)	Max. θ_{inc}	ε_r	*h* (mm)	*P* (λ_o)
[13]	Random	5.4 - 7.4	31.2	45°	2.65	3	0.17
[18]	AMC	5.9 - 12.7	73	N.A.	3.55	4.8	0.33
[19]	Gradient	11.9 -18.3	42.3	N.A.	2.65	3	0.24
[26]	Random	6.9 - 9.2	28.3	40°	2.65	2	0.26
[34]	Aperiodic	9.3 - 15.5	50	30°	2.2	3.3	0.1
[35]	Chessboard	14.5 - 21.8	40.2	40°	10.2	1.27	0.24
[36]	Chessboard	8 – 15.8	68.6	15°	2.2	3.17	0.6
[37]	Staggered	9 - 16	56	N.A.	2.65	2	0.24
[38]	Coding	3.9 - 4.05	3.8	N.A.	110	2	0.26
[39]	Random	9 - 10.8	18.2	N.A.	2.7	2.17	0.2
[40]	Gradient	9.9 - 19.8	66.7	N.A.	2.65	3	0.26
[41]	Chessboard	7 - 13	60	30°	2.2	6.35	0.5
[42]	FSS	6.25 - 12	63	N.A.	2.94	1.52	0.4
This Work	**Fourier**	**10 - 24**	**82.3**	**60°**	**4.4**	**2**	**0.26**

Conclusion

In summary, the CP Fourier phased metasurfaces for RCS reduction are proposed in this letter. The proposed metasurfaces were designed using direct technique based on the Fourier phase formula for the calculations of the phase distribution. The proposed metasurfaces were designed without the need for any complicated or time-consuming algorithms and achieved an RCS reduction bandwidth of 82.3% which is wider than other metasurfaces in the literature. The RCS reduction behaviors can hold under oblique incidence of EM wave at angles up to 60°. Both simulated and measured results confirmed the excellent RCS reduction performance of the Fourier metasurfaces and the proposed design approach. The proposed design approach is very useful in applications when both monostatic and bistatic RCS reductions are required.

REFERENCES

[1] M. K. T. Al-Nuaimi *et al*., "Coding Engineered Reflector for Wide-Band RCS Reduction Under Wide Angle of Incidence," in *IEEE Transactions on Antennas and Propagation*, vol. 70, no. 10, pp. 9947-9952, Oct. 2022.

[2] Y. Qi, B. Zhang, C. Liu and X. Deng, "Ultra-Broadband Polarization Conversion Meta-Surface and its Application in Polarization Converter and RCS Reduction," *IEEE Access*, vol. 8, pp. 116675-116684, 2020.

[3] G. -Y. Deng *et al*., "Ultrabroadband RCS Reduction Design by Exploiting Characteristic Complementary Polarization Conversion Metasurfaces," *IEEE Transactions on Antennas and Propagation*, vol. 70, no. 4, pp. 2904-2914, April 2022.

[4] T. Hong, S. Wang, Z. Liu and S. Gong, "RCS Reduction and Gain Enhancement for the Circularly Polarized Array by Polarization Conversion Metasurface Coating," *IEEE Antennas and Wireless Propagation Letters*, vol. 18, no. 1, pp. 167-171, Jan. 2019.

[5] K. -Y. Liu, G. -M. Wang, T. Cai, H. -P. Li and T. -Y. Li, "Conformal Polarization Conversion Metasurface for Omni-Directional Circular Polarization Antenna Application," *IEEE Transactions on Antennas and Propagation*, vol. 69, no. 6, pp. 3349-3358, June 2021.

[6] M. He *et al*., "Metasurface-Based Wide-Angle Beam Steering for Optical Trapping," *IEEE Access*, vol. 8, pp. 37275-37280, 2020.

[7] M. K. T. Al-Nuaimi and W. Hong, "Discrete dielectric reflectarray and lens for E-band with different feed," *IEEE Antennas and Wireless Propagation Letters*, vol. 13, pp. 947-950, 2014.

[8] M. K. T. Al-Nuaimi, A.-E. Mahmoud, W. Hong, and Y. He, "Design of single-layer circularly polarized reflectarray with efficient beam scanning,'' *IEEE Antennas and Wireless Propagation Letters*, vol. 19, no. 6, pp. 1002-1006, Jun. 2020.

[9] C. Y. Tay *et al*., "Single-Layer Dual-Band Microwave Metasurface Cloak of Conducting Cylinder," *IEEE Transactions on Antennas and Propagation*, vol. 67, no. 6, pp. 4286-4290, June 2019.

[10] H. X. Xu *et al.*, "Polarization-insensitive 3D conformal-skin metasurface cloak," Light: Science & Applications vol. 10, Article number: 75, 2021.

[11] M. K. T. Al-Nuaimi *et al.*, "Backscattered EM-wave manipulation using low cost 1-bit reflective surface at W-band," *Journal of Physics D: Applied Physics*, vol. 51, 2018.

[12] Y. Zheng et al., "Shared Aperture Metasurface With Ultra-Wideband and Wide-Angle Low-Scattering Performance," *Optical Materials Express*, vol. 7, issue 8, pp. 2706-2714, 2017.

[13] X. Liu, J. Gao, L. Xu, X. Cao, Y. Zhao, and S. Li, "A Coding Diffuse Metasurface for RCS Reduction," *IEEE Antennas and Wireless Propagation Letters*, vol. 16, pp. 724–727, 2017.

[14] H. Sun, C. Gu, X. Chen, Z. Li, L. Liu, B. Xu, and Z. Zhou, "Broadband and broad-angle polarization-independent metasurface for radar cross section reduction," *Sci. Rep.*, vol. 7, no. 1, Feb. 2017, Art. no. 407821.

[15] Y. Tian, X. Jing, H. Yu, H. Gan, C. Li, and Z. Hong, "Manipulation of the arbitrary scattering angle based on all-dielectric transmissive Pancharatnam Berry phase coding metasurfaces in the visible range,"*Opt. Exp.*, vol. 28, no. 21, pp. 32107-32123, 2020.

[16] M. K. T. Al-Nuaimi, W. Hong, and Y. He, "Design of Diffusive Modified Chessboard Metasurface," *IEEE Antennas and Wireless Propagation Letters*, vol. 18, no. 8, pp. 1621-1625, Aug. 2019.

[17] K. Li, Y. Liu, Y. Jia, and Y. J. Guo, "A Circularly Polarized High-Gain Antenna with Low RCS Over a Wideband Using Chessboard Polarization Conversion Metasurfaces," *IEEE Transactions on Antennas and Propagation*, vol. 65, no. 8, pp. 4288-4292, Aug. 2017.

[18] M. Mighani and G. Dadashzadeh, "Broadband RCS reduction using a novel double layer chessboard AMC surface," *Electronics Letters*, vol. 52, no. 14, pp. 1253-1255, 2016.

[19] M. Feng, Y. Li, Q. Zheng, J. Zhang, Y. Han, J. Wang, H. Chen, S. Sai, H. Ma, and S. Qu, "Two-dimensional coding phase gradient metasurface for RCS reduction," *J. Phys. D, Appl. Phys.*, vol. 51, no. 37, Sep. 2018.

[20] T. J. Cui, M. Q. Qi, X. Wan, J. Zhao, and Q. Cheng, "Coding Metamaterials, Digital Metamaterials and Programmable Metamaterials," Light: Science and Applications 3, 2014.

[21] T. J. Cui *et al.*, "Information Metamaterials and Metasurfaces," *Journal of Materials Chemistry C* 5, 2017.

[22] M. K. T. Al-Nuaimi, W. Hong and W. G. Whittow, "Aperiodic Sunflower-Like Metasurface for Diffusive Scattering and RCS Reduction," *IEEE Antennas and Wireless Propagation Letters*, vol. 19, no. 7, pp. 1048-1052, July 2020.

[23] F. Yuan, H. Xu, X. Jia, G. Wang and Y. Fu, "RCS Reduction Based on Concave/Convex-Chessboard Random Parabolic-Phased Metasurface," *IEEE Transactions on Antennas and Propagation*, vol. 68, no. 3, pp. 2463-2468, March 2020.

[24] Y. Saifullah, A. B. Waqas, G.-M. Yang, F. Zhang, and F. Xu, "4-bit optimized coding metasurface for wideband RCS reduction," *IEEE Access*, vol. 7, pp. 122378-122386, 2019.

[25] H. Hao, S. Du, and T. Zhang, "Small-size broadband coding metasurface for RCS reduction based on particle swarm optimization algorithm," *Prog. Electromagn. Res. M*, vol. 81, pp. 97-105, 2019.

[26] X. Han, H. Xu, Y. Chang, M. Lin, Z. Wenyuan, X. Wu, and X. Wei, "Multiple diffuse coding metasurface of independent polarization for RCS reduction," *IEEE Access*, vol. 8, pp. 162313-162321, 2020.

[27] H. X. Xu et al, "Deterministic Approach to Achieve Broadband Polarization-Independent Diffusive Scatterings Based on Metasurfaces," *ACS Photonics*, vol.5, pp. 1691-1702, 2018.

[28] X. G. Luo *et al.*, "Recent advances of wide-angle metalenses: principle, design, and applications," *Nanophotonics*, vol. 11, no. 1, pp. 1-20, 2022.

[29] W. Liu et al., "Metasurface enabled wide-angle Fourier lens", *Adv. Mater.*, vol. 30, no. 23, 2018.

[30] S. B. Wang *et al.*, "Ultrathin Dual-Band Wide-Angle Beam Scanning MetalensBased on High-Efficiency Meta-Atom," Adv. Photonics Res., vol 3,3, pp. 2100186 – 2100195, 2022.

[31] J. Y. Yin *et al.*, "Ultra Wideband Polarization-Selective Conversions of Electromagnetic Waves by Metasurface under Large-Range Incident Angles," *Scientific Reports*, vol. 5, Article number: 12476, 2015.

[32] S. Pancharatnam, "Generalized theory of interference and its applications," *Proc. Indian Acad. Sci. A*, vol. 44, no. 6, pp. 398-417, 1956.

[33] C. A. Balanis, Antenna Theory, Analysis and Design, 2nd edition, Wiley, New York, 1996.

[34] A. Edalati and K. Sarabandi, "Wideband, wide angle, polarization independent RCS reduction using nonabsorptive miniaturized-element frequency selective surfaces," *IEEE Transactions on Antennas and Propagation*, vol. 62, pp. 747-754, 2014.

[35] J. C. I. Galarregui, *et al.*, "Broadband radar cross-section reduction using AMC technology," *IEEE Transactions on Antennas and Propagation*, vol. 61, pp. 6136-6143, 2013.

[36] S. H. Kim and Y. J. Yoon, "Wideband radar cross-section reduction on checkerboard metasurfaces with surface wave suppression," *IEEE Antennas and Wireless Propagation Letters*, vol. 18, no. 5, 2019.

[37] J. Liu, J. Li, and S. Zhou, "Polarization Conversion Metamaterial Surface with Staggered-Arrangement Structure for Broadband Radar Cross Section Reduction," *IEEE Antennas and Wireless Propagation Letters*, vol. 18, no. 5, May 2019.

[38] L. Shao, M. Premaratne and W. Zhu, "Dual-Functional Coding Metasurfaces Made of Anisotropic All-Dielectric Resonators," *IEEE Access*, vol. 7, pp. 45716-45722, 2019

[39] Y. Zhuang, G. Wang, J. Liang, T. Cai, W. Guo, and Q. Zhang, "Flexible and polarization-controllable diffusion metasurface with optical transparency," J. Phys. D, Appl. Phys., vol. 50, no. 46, Nov. 2017, Art. no. 465102.

[40] Q. Zheng, Y. Li, J. Zhang, H. Ma, J. Wang, Y. Pang, Y. Han, S. Sui, Y. Shen, H. Chen, and S. Qu, "Wideband, wide-angle coding phase gradient metasurfaces based on Pancharatnam-Berry phase," *Sci. Rep.*, vol. 7, Mar. 2017, Art. no. 43543.

[41] A. Ghayekhloo, M. Afsahi, and A. A. Orouji, "Checkerboard plasma electromagnetic surface for wideband and wide-angle bistatic radar cross section reduction," *IEEE Trans. Plasma Sci.*, vol. 45, no. 4, pp. 603–609, Apr. 2017.

[42] M. Pazokian, N. Komjani and M. Karimipour, "Broadband RCS Reduction of Microstrip Antenna Using Coding Frequency Selective Surface," *IEEE Antennas and Wireless Propagation Letters*, vol. 17, no. 8, pp. 1382-1385, Aug. 2018.